ACS APPLIED MATERIALS & INTERFACES

Research Article

www.acsami.org

Enhancement of Light Emission from Silicon by Precisely Tuning Coupled Localized Surface Plasmon Resonance of a Nanostructured Platinum Layer Prepared by Atomic Layer Deposition

Chung-Ting Ko,[†] Yin-Yi Han,[‡,§] Wei-Cheng Wang,[†] Jay Shieh,[†] and Miin-Jang Chen*,[†,⊥]

[†]Department of Materials Science and Engineering, National Taiwan University, No. 1, Section 4, Roosevelt Road, Taipei 10617 Taiwan

[‡]Department of Traumatology, Surgery, and Anesthesia, National Taiwan University Hospital, Taipei 10002, Taiwan

[§]Graduate Institute of Biomedical Electronic and Bioinformatic, National Taiwan University Taipei 10617, Taiwan

[⊥]National Nano Device Laboratories, Hsinchu 30078, Taiwan

ABSTRACT: Plasmonic enhancement of photoluminescence from bulk silicon was achieved by spectrally tailoring coupled localized surface plasmon resonance (LSPR) in the Al_2O_3 cover/nanostructured platinum (nano-Pt)/Al_2O_3 spacer/silicon multilayer structures prepared by atomic layer deposition (ALD). Agreement between the simulation and experimental data indicates that the plasmonic activity originates from absorption enhancement due to coupled LSPR. Because of the optimized dielectric environment deposited by ALD around the nano-Pt layer, absorption of the multilayer structure was enhanced by the precise tuning of coupled LSPR to coincide with the excitation wavelength. This accurate plasmonic multilayer structure grown by ALD with high precision, tunability, uniformity, and reproducibility can be further applied in efficient light-emitting devices.

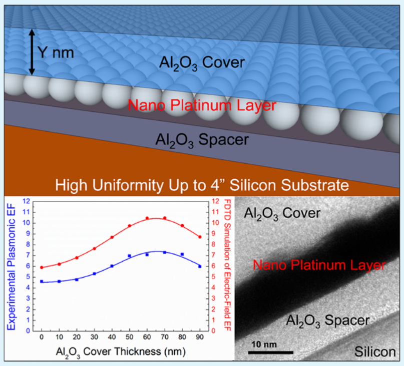

KEYWORDS: *atomic layer deposition, plasmonics, localized surface plasmon resonance, surface-enhanced luminescence, metal-enhanced fluorescence, silicon*

INTRODUCTION

Because silicon (Si) is the most dominant material for ultralarge-scale integrated circuits, the monolithic integration of microelectronic and photonic devices in a single Si chip has attracted considerable attention for high-speed optical interconnection.[1−7] However, few Si-based light-emitting devices have been able to realize practical applications. In bulk Si, where radiative transition is a phonon-assisted process due to an indirect band gap, nonradiative recombination proceeds much faster than radiative recombination, accordingly resulting in a very low quantum efficiency (10^{-6}) of light emission from bulk Si. In order to improve the light emission efficiency of Si-based light-emitting diodes (LEDs), nonradiative recombination has to be suppressed to a low level both in bulk and at the surface. Nonradiative recombination in bulk can be minimized by using high-quality Si substrates, including those grown by the float zone or magnetically confined Czochralski (CZ) method.[8] Surface recombination can be reduced by depositing a surface passivation layer. In our previous investigation, a thin Al_2O_3 surface passivation layer prepared by atomic layer deposition (ALD) at a low temperature was demonstrated to be instrumental in enhancing light emission from bulk Si.[9]

Apart from the efforts to reduce nonradiative recombination, the light emission efficiency from Si can be enhanced based on the Purcell effect that modifies the photonic density of states near the metallic nanostructures. An 8-fold enhancement of electroluminescence was obtained from Si-on-insulator LEDs at $\lambda = 900$ nm by excitation of the surface plasmon resonance in silver nanoparticles, as demonstrated by Pillai et al.[10] The enhancement results from coupling with localized surface plasmons, which offer an additional radiative decay route via the metallic nanostructures. On the other hand, because the electric field is concentrated in a local area, such as hotspots between metallic nanostructures due to the dipole−dipole coupling,[11] absorption of the light emitter can be significantly enhanced according to Fermi's golden rule. Plasmonic enhancement of the photon−matter interaction provides a new way to manipulate the photons at the subwavelength scale and hence enables a broad variety of applications including plasmonic enhancement of light absorption, emission, and Raman scattering.[12,13]

Recently, the remarkable progress in the fabrication of metallic nanostructures contributes to significant advances in plasmonics. The chemical synthesis of gold and silver nanoparticles is the most popular method to fabricate metallic nanostructures.[14−16] Vacuum deposition techniques including

Received: December 18, 2013
Accepted: February 24, 2014
Published: February 24, 2014

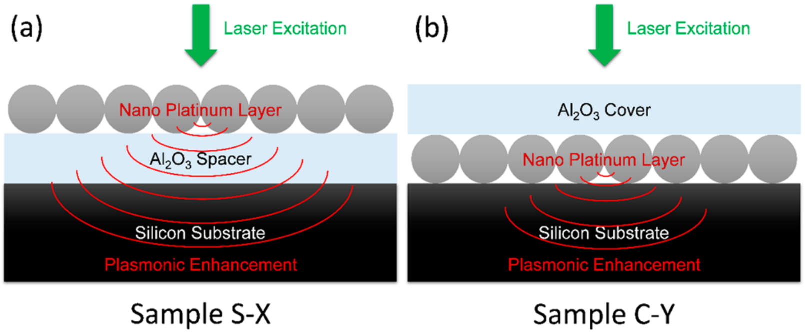

Figure 1. Schematic diagrams of the (a) nano-Pt/Al_2O_3 spacer/Si and (b) Al_2O_3 cover/nano-Pt/Si multilayer structures.

evaporation and sputtering have also been applied to produce metallic nanostructures on a substrate.[17] On the other hand, electron-beam lithography and focused-ion milling have been extensively used to fabricate metallic nanostructures of miscellaneous sizes and shapes.[18,19] However, these nanofabrication techniques are usually restrained by low uniformity, throughput, and reproducibility. ALD is another prospective technique for fabricating high-quality plasmonic nanostructures because of many benefits such as accurate thickness control, conformal step coverage, excellent uniformity, low defect density, and good reproducibility, as a result of the self-limiting and layer-by-layer growth.[20−25] Because the localized surface plasmon resonance (LSPR) can be spectrally tuned by engineering the dielectric environment of the plasmonic nanostructures, the "digital" growth of the surrounding dielectrics around the metallic nanostructures by ALD offers an accurate way to tailor the LSPR wavelength.[26,27]

However, the ALD processes for conventional plasmonic materials such as gold and silver are not mature. By contrast, the ALD process for platinum (Pt) has been well established.[28] Furthermore, because the Pt nanostructures are of great interest for catalysis because of their high chemical potential and large surface area,[29] Pt is quite an attractive material in plasmonics and LSPR-enhanced photocatalysis for further research. Our previous study has demonstrated giant enhancement of light emission in the ultraviolet (UV) region as large as 2 orders of magnitude from nanoscale ZnO thin films by the plasmonic activity of the nanostructured Pt layer.[30] In this paper, the plasmonic Al_2O_3 cover/nanostructured Pt (nano-Pt)/Al_2O_3 spacer/Si multilayer structure was applied to enhance light absorption and emission of Si, leading to an increase of the light emission efficiency from bulk Si in the IR spectrum. The plasmonic activity was provided by the coupled LSPR in the nano-Pt layer. The nanoscale Al_2O_3 and nano-Pt layers were engineered "digitally" in a precise and well-controlled manner by ALD. Therefore, the spectral peak of coupled LSPR can be accurately tailored by the Al_2O_3 thickness around the nano-Pt layer to spectrally overlap with the excitation wavelength. In addition, the self-limiting growth and wide process window of ALD are beneficial to the fabrication of plasmonic nanostructures with high accuracy and reproducibility with wafer-scale uniformity. A 7.2-fold plasmonic enhancement of photoluminescence (PL) from bulk Si was achieved at $\lambda = 1140$ nm with high uniformity up to a 4-in. substrate.

■ EXPERIMENTAL SECTION

Figure 1 shows the schematic diagrams of the nano-Pt/Al_2O_3 spacer/Si and Al_2O_3 cover/nano-Pt/Si multilayer structures. The p-type CZ Si substrate acts as the light emitter in this study. All of the layers upon the Si substrate were deposited by the thermal ALD system (Savannah 100, Cambridge Nanotech, Cambridge, MA). The Al_2O_3 layers were prepared at 180 °C, using trimethylaluminum [$Al(CH_3)_3$] and H_2O vapor as the precursors. Trimethyl(methylcyclopentadienyl)platinum(IV) [$(MeCp)PtMe_3$] and oxygen were used to grow the nano-Pt layer at 270 °C. First, an Al_2O_3 spacer layer was deposited on the Si substrate. Next, 100 ALD cycles were applied to deposit the nano-Pt layer on the Al_2O_3 spacer. During the initial growth stage with a few ALD cycles, the discrete Pt nanoclusters appeared on the surface.[28,31−33] These Pt nanoclusters would not coalesce together to form a continuous film if the Pt layer is not of sufficient thickness, resulting in the formation of a nanostructured Pt layer. Afterward, an Al_2O_3 cover layer was deposited on the nano-Pt layer. The thickness of Al_2O_3 and the morphology of the nano-Pt layers can be accurately and "digitally" controlled by the number of applied ALD cycles. The plasmonic multilayer structures without the Al_2O_3 cover layer, as shown in Figure 1a, were denoted as S-*X* according to the Al_2O_3 spacer thickness of *X* nm. Another group of samples without the Al_2O_3 spacer (Figure 1b) were designated as C-*Y*, in which *Y* stands for the thickness of the Al_2O_3 cover layer (in nanometers). In order to obtain the plasmonic EF of PL, the reference samples, named as S-*X*-R, were also prepared. All of the thickness of each layer and the process conditions of the reference samples S-*X*-R were the same as those of each corresponding S-*X* samples, except that the nano-Pt layer was not grown in the reference samples.

The cross section of Al_2O_3 cover/nano-Pt/Al_2O_3 spacer/Si multilayer structures and the thickness of each layer were characterized by high-resolution transmission electron microscopy (HRTEM; JEOL JEM-2100F). The sample for cross-sectional HRTEM measurement was prepared by a focused-ion beam (FEI NOVA-200 NanoLab Compatible). The surface morphology of the nano-Pt layer was examined by scanning electron microscopy (SEM; FEI NOVA NanoSEM 450). The plasmonic multilayer structures were excited by a continuous-wave diode-pumped solid-state laser at $\lambda = 532$ nm to measure the PL spectra. A spectrophotometer (Avantes AvaSpec-2048L) with an integrated sphere was used to probe the absorbance spectra of the plasmonic multilayer structures. The effective minority carrier lifetime in Si covered with the multilayer structure was measured by the quasi-steady-state photoconductance (QSSPC) technique using a Sinton WCT-120 lifetime tester. The refractive index and extinction coefficients of the multilayer structures were extracted by a spectroscopic ellipsometer (Ellipso Technology Elli-SE) at $\lambda = 633$ nm.

■ RESULTS AND DISCUSSION

Figure 2a shows the cross-sectional HRTEM image of sample S-10 with an Al_2O_3 cover layer. The thicknesses of the Al_2O_3 spacer, nano-Pt, and Al_2O_3 cover layers are 10.2, 10.6, and 15.1 nm, respectively. The thickness of each layer is in good agreement with the estimation according to applied ALD cycles, revealing the excellent thickness controllability of ALD. The undulation between the nano-Pt and Al_2O_3 cover layers suggests that the Pt nanoclusters are bundled together to form

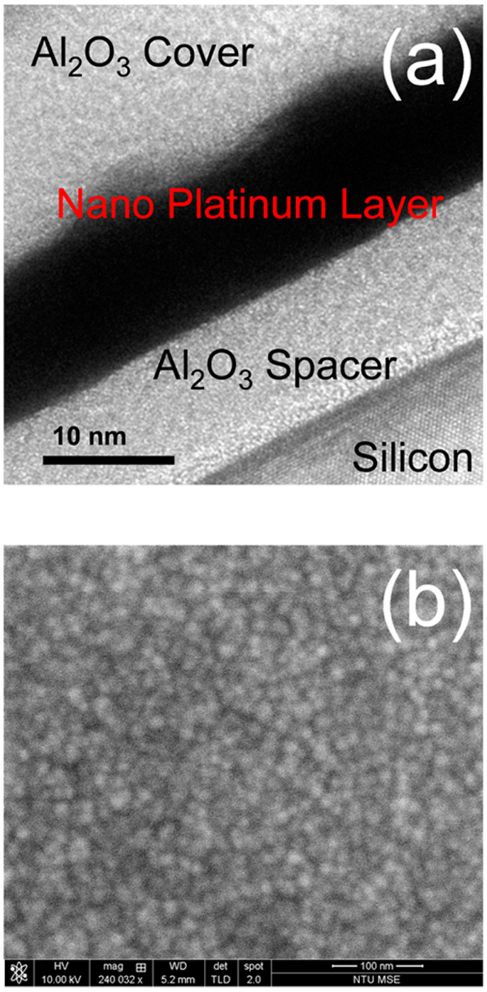

Figure 2. (a) Cross-sectional HRTEM image of sample S-10 with a 15 nm Al_2O_3 cover layer. (b) SEM image of the nano-Pt layer.

the nano-Pt layer. The SEM surface morphology of the nano-Pt layer without the Al_2O_3 cover layer is shown in Figure 2b, revealing the presence of uniformly dispersed Pt nanoclusters of an average diameter of about 10 nm (which is close to the SEM resolution). Because of the great difference between the surface energy of Al_2O_3 and Pt, the growth of the nanoscale Pt layer follows the Volmer−Weber mode, and it aggregates to form the Pt nanoclusters at the initial stage of ALD.[31] The observation of Pt nanocluster growth at the initial few ALD cycles is consistent with the results reported by Novak et al.,[34] Aaltonen et al.,[28] and Baker et al.[31]

In this study, the plasmonic EF deduced from the measured PL intensity was calculated using the following methodology. In the nano-Pt/Al_2O_3 spacer/Si multilayer structure (S-X samples), four factors influencing the PL intensity are considered: (1) plasmonic enhancement by the LSPR in the nano-Pt layer, (2) surface passivation due to the Al_2O_3 spacer on the Si, (3) attenuation of light passing through the nano-Pt layer, and (4) interference within the multilayer structure. The measured PL intensities of the S-X and S-X-R samples are denoted as $PL_{S\text{-}X}$ and $PL_{S\text{-}X\text{-}R}$, which can be expressed as

$$PL_{S\text{-}X} = I_0 T_X^{Pt} \alpha \eta EF_X^{Pt} t_X^{Pt}$$

$$PL_{S\text{-}X\text{-}R} = I_0 T_X \alpha \eta t_X$$

where I_0 is the intensity incident laser beam at $\lambda = 532$ nm, T_X^{Pt} and T_X represent the overall transmission coefficients of the incident laser beam passing from the top through the S-X and S-X-R multilayers into Si, and t_X^{Pt} and t_X are the overall transmission coefficients of the light emission from Si at $\lambda = 1140$ nm passing through the S-X and S-X-R multilayer into the air, respectively. EF_X^{Pt} is the plasmonic EF as a result of LSPR in the nano-Pt layer at a spacer thickness equal to X nm. α and η are the absorption coefficient and light emission efficiency of Si without plasmonic enhancement. Surface passivation by the Al_2O_3 spacer leads to the increment of η due to suppression of the surface recombination, as a result of reduction in the interfacial state density or a decrease in the minority carrier concentration near the interface ascribed to the electric field built by fixed oxide charges in the Al_2O_3 spacer.[35−37]

The effects of optical attenuation by the nano-Pt layer and interference within the multilayer are included in the overall transmission coefficients T_X^{Pt}, T_X, t_X^{Pt}, and t_X, which were calculated by the finite difference time domain (FDTD; *Solutions 8.6*, Lumerical Solutions Inc., Vancouver, British Columbia, Canada) method. The Drude−Lorentz model was used to describe the dielectric function of Pt. The morphology of the nano-Pt layer was depicted as randomly arranged nanoparticles by the built-in function "uniform random particle distribution", with 10000 nanoparticles distributed in a 500 nm × 500 nm × 10 nm space. The particle diameter was set with the range from 8 to 10 nm, which is close to those shown in the HRTEM and SEM images. In order to truncate the computational domain, the simulation was performed with the periodic boundary condition in the horizontal direction and the perfectly matched layers in the vertical direction. The Yee-cell size was selected as 0.25 nm^3. A total-field/scattered-field plane wave was used to introduce the incident laser beam. Because the electromagnetic field near the plasmonic nanostructure evanesces exponentially with a decay length on the order of 10 nm,[38−40] it is assumed that no plasmonic enhancement exists in sample S-70, in which the spacer thickness is as large as 70 nm. The measured intensities $PL_{S\text{-}70}$ and $PL_{S\text{-}70\text{-}R}$ of the S-70 and S-70-R samples are given by

$$PL_{S\text{-}70} = I_0 T_{X=70}^{Pt} \alpha \eta t_{X=70}^{Pt} (EF_{X=70}^{Pt} = 1)$$

$$PL_{S\text{-}70\text{-}R} = I_0 T_{X=70} \alpha \eta t_{X=70}$$

The ratio of $PL_{S\text{-}70}$ to $PL_{S\text{-}70\text{-}R}$ is

$$\frac{PL_{S\text{-}70}}{PL_{S\text{-}70\text{-}R}} = \frac{T_{X=70}^{Pt} t_{X=70}^{Pt}}{T_{X=70} t_{X=70}}$$

which contains information of optical attenuation by the nano-Pt layer and interference within the multilayer without plasmonic enhancement ($EF_{X=70}^{Pt} = 1$). On the other hand, the ratio of PL_{S-X} to $PL_{S\text{-}X\text{-}R}$

$$\frac{PL_{S\text{-}X}}{PL_{S\text{-}X\text{-}R}} = EF_X^{Pt} \frac{T_X^{Pt} t_X^{Pt}}{T_X t_X}$$

involves plasmonic enhancement, optical attenuation by the nano-Pt layer, as well as interference within the multilayer with the X nm Al_2O_3 spacer. Then plasmonic EF_X^{Pt} can be obtained according to the following expression:

$$\frac{\dfrac{\mathrm{PL}_{\text{S-}X}}{\mathrm{PL}_{\text{S-}X\text{-R}}}}{\dfrac{\mathrm{PL}_{\text{S-70}}}{\mathrm{PL}_{\text{S-70-R}}}} = \mathrm{EF}_X^{\mathrm{Pt}} \frac{\dfrac{T_X^{\mathrm{Pt}} t_X^{\mathrm{Pt}}}{T_X t_X}}{\dfrac{T_{X=70}^{\mathrm{Pt}} t_{X=70}^{\mathrm{Pt}}}{T_{X=70} t_{X=70}}} \tag{1}$$

where the factor $(\mathrm{PL}_{\text{S-}X}/\mathrm{PL}_{\text{S-}X\text{-R}})/(\mathrm{PL}_{\text{S-70}}/\mathrm{PL}_{\text{S-70-R}})$ was obtained from the measured PL intensities and $(T_X^{\mathrm{Pt}} t_X^{\mathrm{Pt}}/T_X t_X)/(T_{X=70}^{\mathrm{Pt}} t_{X=70}^{\mathrm{Pt}}/T_{X=70} t_{X=70})$ can be calculated by the FDTD method. Because the optical attenuation coefficient of the nano-Pt layer is divided out in the factor $(T_X^{\mathrm{Pt}} t_X^{\mathrm{Pt}}/T_X t_X)/(T_{X=70}^{\mathrm{Pt}} t_{X=70}^{\mathrm{Pt}}/T_{X=70} t_{X=70})$, the actual value of the optical attenuation is not important in the calculation of plasmonic EF.

Figure 3 shows the experimental plasmonic EF ($\mathrm{EF}_X^{\mathrm{Pt}}$, blue line) deduced from the measured PL intensity of each sample and eq 1 as a function of the Al_2O_3 spacer thickness X ranging from 0 to 70 nm, with an interval of 1 nm (from 0 to 10 nm) and 5 nm (from 10 to 45 nm). The inset of Figure 3 shows the typical room-temperature PL spectrum from the multilayer structure, with a spectral peak around 1140 nm corresponding to the transverse optical phonon-assisted interband transition in Si. With an increase of the Al_2O_3 spacer thickness from 0 to 70 nm, $\mathrm{EF}_X^{\mathrm{Pt}}$ drops rapidly and gradually approaches 1 when the spacer thickness is greater than 10 nm. A 4.6-fold plasmonic EF of PL was observed, with the nano-Pt layer directly contacting with Si. Figure 3 also shows FDTD simulation of the average electric-field EF at $\lambda = 532$ nm (red line) in Si within the region between the Al_2O_3 spacer/Si interface and 10 nm depth underneath the interface. In this simulation, the dielectric function and morphology of the nano-Pt layer and the boundary conditions of the computational domain are the same as those mentioned above. Because the distance between the nano-Pt layer and Si is up to 70 nm in sample S-70 in which the plasmonic EF can be assumed to be 1, FDTD simulation of the average electric-field EF shown in Figure 3 was obtained by normalizing the average electric-field intensity of each sample to that of sample S-70. In addition, the Purcell factor obtained by FDTD simulation shows that no enhancement occurs at $\lambda = 1140$ nm. Therefore, the excellent agreement between the experimental plasmonic EF and FDTD simulation of the average electric-field EF at $\lambda = 532$ nm, as shown in Figure 3, clearly indicates that plasmonic enhancement can be attributed to absorption enhancement due to the LSPR in the nano-Pt layer. The rapid decrease of the plasmonic EF with the Al_2O_3 spacer thickness can be deduced from the exponential decay of the electric field with the distance between the nano-Pt layer and Si. Because the coupling to the high-order LSPR modes is quite limited under the condition of low Purcell enhancement, the quenching in plasmonic PL enhancement was not observed in Figure 3 because the nano-Pt layer is close to the bulk Si light emitter.

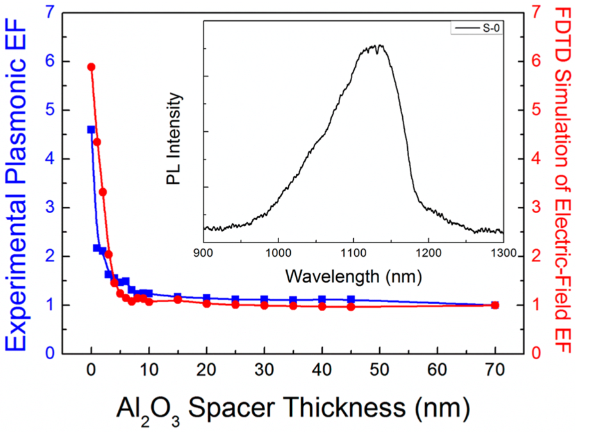

Figure 3. Experimental plasmonic EF (blue line) and FDTD simulation of the average electric-field EF (red line) of the S-X sample as a function of the Al_2O_3 spacer thickness. The inset shows the typical room-temperature PL spectrum from the plasmonic multilayer structure.

On the other hand, in order to elucidate the effect of chemical enhancement resulting from charge transfer between the nano-Pt layer and Si, the minority carrier lifetime in the S-X sample was examined by the QSSPC method.[41] It is expected that charge transfer between the nano-Pt layer and Si may result in variation of the minority carrier lifetime. Figure 4 shows the minority carrier lifetime as a function of the Al_2O_3 spacer thickness. With an increase of the Al_2O_3 spacer thickness from 0 to 70 nm, the minority carrier lifetime increases rapidly from ~2 μs and reaches a maximum of about 10 μs at a spacer thickness of 10 nm. Then the minority carrier lifetime drops with the Al_2O_3 spacer thickness and approaches a constant value close to 5 μs when the spacer thickness is greater than 30 nm. The variation trend of the minority carrier lifetime with the Al_2O_3 spacer thickness is completely different from that of plasmonic EF shown in Figure 3. Thus, one can deduce that enhancement does not originate from charge transfer between the nano-Pt layer and Si (chemical enhancement). The Al_2O_3 thickness dependence of the minority carrier lifetime shown in Figure 4 is consistent with the previous works reported by Sun et al.[42] and Saint-Cast et al.[43] When the Al_2O_3 spacer thickness is below 10 nm, an increase of the minority carrier lifetime with the spacer thickness can be attributed to a decrease in the interfacial state density, i.e., the so-called chemical passivation effect. On the other hand, the presence of a net positive oxide charge in the Al_2O_3 layer can account for a decrease of the minority carrier lifetime with a spacer thickness greater than 10 nm, due to an increase in the minority carrier (electron) concentration in p-type Si near the interface caused by a positive oxide charge in Al_2O_3.[44,45]

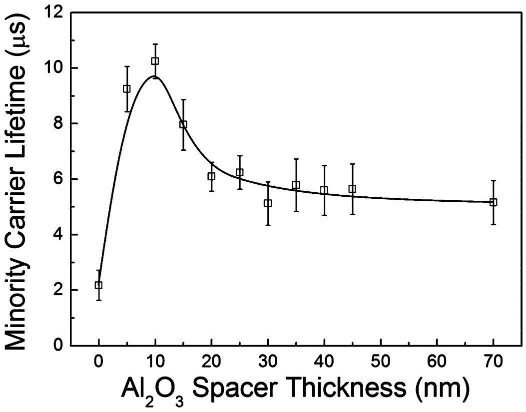

Figure 4. Minority carrier lifetime of the S-X sample as a function of the Al_2O_3 spacer thickness.

From Figure 3, one can see that the plasmonic EF decays significantly with increasing Al_2O_3 spacer thickness and maximum plasmonic enhancement was achieved when the nano-Pt layer is in direct contact with Si. Because the plasmonic EF can further increase if the LSPR could spectrally match the excitation laser wavelength, an Al_2O_3 cover layer was introduced on top of the nano-Pt layer to tune the LSPR wavelength. Figure 5 shows the plasmonic EF deduced from the measured PL intensities (blue line) and FDTD simulation of the average electric-field EF (red line) in the C-0, C-10, ..., C-90 samples, in which the thickness of the Al_2O_3 cover layer ranges from 0 to 90 nm. The measured PL intensities of the C-Y and C-0 samples, as denoted by $PL_{C\text{-}Y}$ and $PL_{C\text{-}0}$, can be expressed by

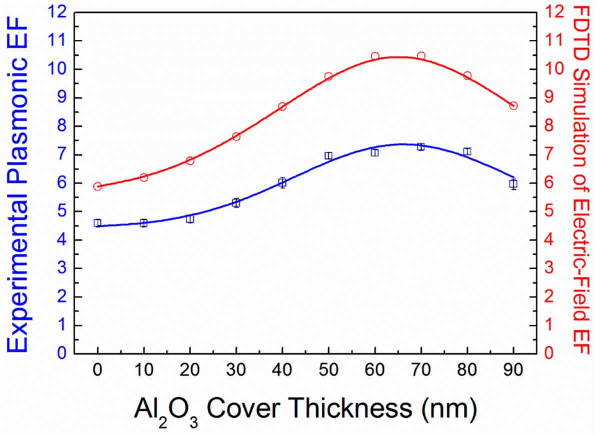

Figure 5. Experimental plasmonic EF (blue line) and FDTD simulation of the average electric-field EF (red line) as a function of the Al_2O_3 cover thickness.

$$PL_{C\text{-}Y} = I_0 T_Y^{Pt} \alpha\eta EF_Y^{Pt} t_Y^{Pt}$$

$$PL_{C\text{-}0} = I_0 T_{Y=0}^{Pt} \alpha\eta EF_{Y=0}^{Pt} t_{Y=0}^{Pt}$$

Similarly, the FDTD method was used to calculate the overall transmission coefficients T_Y^{Pt}, t_Y^{Pt}, $T_{Y=0}^{Pt}$, and $t_{Y=0}^{Pt}$. The ratio $PL_{C\text{-}Y}/PL_{C\text{-}0}$ can be used to calculate the plasmonic EF_Y^{Pt}:

$$\frac{PL_{C\text{-}Y}}{PL_{C\text{-}0}} = \frac{EF_Y^{Pt}}{EF_{Y=0}^{Pt}} \frac{T_Y^{Pt} t_Y^{Pt}}{T_{Y=0}^{Pt} t_{Y=0}^{Pt}} \qquad (2)$$

where the optical attenuation of the nano-Pt layer is also divided out in the factor $T_Y^{Pt} t_Y^{Pt}/T_{Y=0}^{Pt} t_{Y=0}^{Pt}$. Because the structures of the S-0 and C-0 samples are exactly the same, the plasmonic EF of C-0 is identical with that of S-0, i.e., $EF_{Y=0}^{Pt} = EF_{X=0}^{Pt} = 4.6$. Therefore, the experimental plasmonic EF can be deduced from the measured PL intensities $PL_{C\text{-}Y}$ and $PL_{C\text{-}0}$ according to eq 2. On the other hand, FDTD simulation of the average electric-field EF was obtained after following the details as mentioned above. It can be seen that the trend of the experimental plasmonic EF (blue line) agrees quite well with that of the simulated electric-field EF (red line). The plasmonic EF reaches a maximum of ~7.2 in the multilayer structure with the ALD-grown nano-Pt layer covered by a 60 nm Al_2O_3 layer.

Maximum plasmonic enhancement, when the thickness of the Al_2O_3 cover layer equals 60 nm, as shown in Figure 5, can be explained as follows. Figure 6 shows the normalized absorbance spectra of the C-0, C-10, ..., C-90 samples obtained from FDTD simulation and measurement, revealing good consistency between the simulation and experimental data. In the simulation, the incident light was introduced by a broadband total-field/scattered-field plane wave with a spectral range from 400 to 1000 nm. In the C-0, C-10, C-20, and C-30 samples, the broad spectral envelope with a slight increase of the absorbance from $\lambda = 400$ to 1000 nm originates from the bulk Si substrate. As for the samples C-40, C-50, ..., C-90, a absorbance peak was clearly observed, which can be deduced from the coupled LSPR between the Pt nanostructures. Generally, the LSPR wavelength of the Pt nanostructures with a feature size of less than 100 nm is usually located in the deep-UV region.[46,47] The coupling of LSPR between the Pt nanostructures leads to a red shift of LSPR to the visible spectrum when polarization of the incident laser beam is parallel to the dipolar near field between the coupled plasmonic nanostructures.[48] Figure 6 also displays that the maximum absorbance wavelength (λ_{max}) of the coupled LSPR gradually red shifts from around 460 to 740 nm with increasing thickness of the Al_2O_3 cover layer. Because the effective refractive index around the nano-Pt layer increases with the thickness of the cover layer because of the higher refractive index of Al_2O_3 than than that air, such a significant red shift of the coupled LSPR λ_{max} can be ascribed to an increase in the effective refractive index of the surrounding dielectric around the nano-Pt layer. The coincidence between the simulation and experimental result, as shown in Figure 6, clearly demonstrates that the coupled LSPR wavelength can be precisely tailored using ALD by "digital" growth of the environmental dielectric around plasmonic nanostructures. It should be noted that the coupled LSPR λ_{max} of sample C-60 is very close to the excitation wavelength at 532 nm, and thus sample C-60 has a maximum absorbance at 532 nm. As seen from Figure 5, maximum PL enhancement also takes place in the plasmonic multilayer structure with an Al_2O_3 cover layer of 60 nm thickness, clearly indicating that the overlap of the coupled LSPR λ_{max} with the excitation wavelength is essential to achieving maximum plasmonic enhancement. On the other hand, it is seen that the coupled LSPR wavelength ranges from ~460 to 740 nm, which is far away from the Si light emission wavelength of 1140 nm. This is responsible for no Purcell enhancement as mentioned above, and so the plasmonic PL EF can be deduced from absorption enhancement as a result of coupled LSPR in the nano-Pt layer.

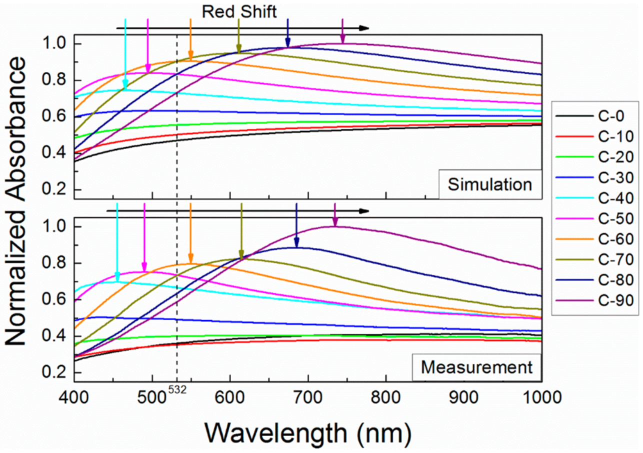

Figure 6. FDTD-simulated and measured absorbance spectra of the C-0, C-10, ..., C-90 samples, where the data were normalized to the maximum absorbance of sample C-90.

Figure 7 shows the uniformity of the nano-Pt layer on a 4-in. Si substrate, in which the pseudo refractive index (n) and extinction coefficient (k) were extracted by the spectroscopic ellipsometer at $\lambda = 532$ nm. The percent nonuniformity can be

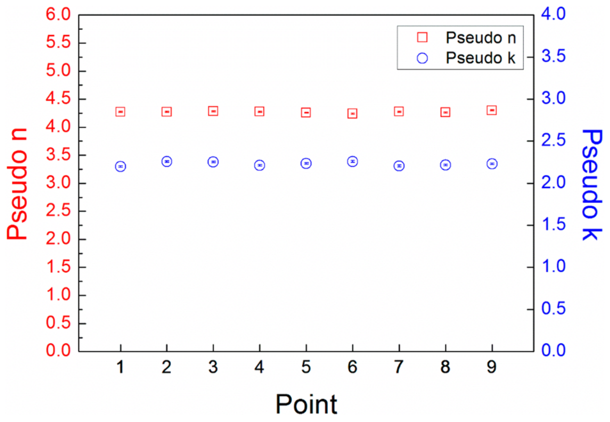

Figure 7. Uniformity of the pseudo-*n* and -*k* of the nano-Pt layer on the Si substrate over a 4-in. substrate.

obtained according to the 9-point map on the 4-in. area using the following formula:

$$\text{percent nonuniformity} = \frac{(\max - \min)/2}{\text{mean}} \times 100$$

Thus, the percent nonuniformities of the pseudo-*n* and -*k* of the nano-Pt layer on Si across the 4-in. wafer are ±0.705% and ±1.318%, respectively. Because the pseudo-*n* and -*k* are sensitive to the thickness and microstructure of the nano-Pt layer, the result reveals high uniformity of the nano-Pt layer prepared by ALD. This wafer-scale uniformity is attributable to self-limiting growth, contributing to insensitivity to the inhomogeneity of the precursors and substrate temperature in the ALD process. Therefore, ALD shows excellent capability for fabricating tunable plasmonic nanostructures with inherent high accuracy, controllability, uniformity, and reproducibility over a large area.

■ CONCLUSION

The ALD technique was used to tailor the coupled LSPR in the Al_2O_3 cover/nano-Pt/Al_2O_3 spacer/Si multilayer structure, to achieve plasmonic enhancement of light emission from Si. The plasmonic activity was supported by the uniformly dispersed nano-Pt layer grown by ALD. Broad-band and precise tuning of the coupled LSPR wavelength was accomplished by engineering the thickness of the dielectric around the nano-Pt layer. FDTD simulation supports the theory that absorption enhancement resulting from the spectral overlap between the coupled LSPR and excitation wavelength contributes to plasmon-enhanced PL. This plasmonic multilayer configuration with high precision, tunability, uniformity, and reproducibility can be used to accurately tune the LSPR to coincide with the optical excitation or light emission wavelengths, for further enhancement of the light emission efficiency in future studies.

■ AUTHOR INFORMATION

Corresponding Author

*E-mail: mjchen@ntu.edu.tw. Tel: +886-2-3366-5301.

Notes

The authors declare no competing financial interest.

■ ACKNOWLEDGMENTS

This work is partially supported by the National Science Council of Taiwan, Republic of China (NSC Grants 102-2325-B-002-013, 102-2628-M-001-008, and 102-2120-M-002-003).

■ REFERENCES

(1) Canham, L. T. Silicon Quantum Wire Array Fabrication by Electrochemical and Chemical Dissolution of Wafers. *Appl. Phys. Lett.* **1990**, *57*, 1046−1048.

(2) Pavesi, L.; Dal Negro, L.; Mazzoleni, C.; Franzo, G.; Priolo, F. Optical gain in silicon nanocrystals. *Nature* **2000**, *408*, 440−444.

(3) Rong, H. S.; Jones, R.; Liu, A. S.; Cohen, O.; Hak, D.; Fang, A.; Paniccia, M. A continuous-wave Raman silicon laser. *Nature* **2005**, *433*, 725−728.

(4) Lu, Z. H.; Lockwood, D. J.; Baribeau, J. M. Quantum Confinement and Light-Emission in SiO_2/Si Superlattices. *Nature* **1995**, *378*, 258−260.

(5) Ng, W. L.; Lourenco, M. A.; Gwilliam, R. M.; Ledain, S.; Shao, G.; Homewood, K. P. An efficient room-temperature silicon-based light-emitting diode. *Nature* **2001**, *410*, 192−194.

(6) Walters, R. J.; Bourianoff, G. I.; Atwater, H. A. Field-effect electroluminescence in silicon nanocrystals. *Nat. Mater.* **2005**, *4*, 143−146.

(7) Palm, J.; Gan, F.; Zheng, B.; Michel, J.; Kimerling, L. C. Electroluminescence of erbium-doped silicon. *Phys. Rev. B* **1996**, *54*, 17603−17615.

(8) Green, M. A.; Zhao, J. H.; Wang, A. H.; Reece, P. J.; Gal, M. Efficient silicon light-emitting diodes. *Nature* **2001**, *412*, 805−808.

(9) Chen, M. J.; Shih, Y. T.; Wu, M. K.; Tsai, F. Y. Enhancement in the efficiency of light emission from silicon by a thin Al_2O_3 surface-passivating layer grown by atomic layer deposition at low temperature. *J. Appl. Phys.* **2007**, *101*, 033130.

(10) Pillai, S.; Catchpole, K. R.; Trupke, T.; Zhang, G.; Zhao, J.; Green, M. A. Enhanced emission from Si-based light-emitting diodes using surface plasmons. *Appl. Phys. Lett.* **2006**, *88*, 161102.

(11) Hayashi, S.; Okamoto, T. Plasmonics: visit the past to know the future. *J. Phys. D: Appl. Phys.* **2012**, *45*, 433001.

(12) Kim, B. H.; Cho, C. H.; Mun, J. S.; Kwon, M. K.; Park, T. Y.; Kim, J. S.; Byeon, C. C.; Lee, J.; Park, S. J. Enhancement of the external quantum efficiency of a silicon quantum dot light-emitting diode by localized surface plasmons. *Adv. Mater.* **2008**, *20*, 3100−3104.

(13) Le, K. Q.; Bienstman, P. Optical Modeling of Plasmonic Nanoparticles Enhanced Light Emission of Silicon Light-Emitting Diodes. *Plasmonics* **2011**, *6*, 53−57.

(14) Rycenga, M.; Cobley, C. M.; Zeng, J.; Li, W. Y.; Moran, C. H.; Zhang, Q.; Qin, D.; Xia, Y. N. Controlling the Synthesis and Assembly of Silver Nanostructures for Plasmonic Applications. *Chem. Rev.* **2011**, *111*, 3669−3712.

(15) Sun, Y. G.; Xia, Y. N. Shape-controlled synthesis of gold and silver nanoparticles. *Science* **2002**, *298*, 2176−2179.

(16) Wiley, B.; Sun, Y. G.; Mayers, B.; Xia, Y. N. Shape-controlled synthesis of metal nanostructures: The case of silver. *Chem.—Eur. J.* **2005**, *11*, 454−463.

(17) Shevchenko, A.; Ovchinnikov, V.; Shevchenko, A. Large-area nanostructured substrates for surface enhanced Raman spectroscopy. *Appl. Phys. Lett.* **2012**, *100*, 171913.

(18) Hicks, E. M.; Zou, S. L.; Schatz, G. C.; Spears, K. G.; Van Duyne, R. P.; Gunnarsson, L.; Rindzevicius, T.; Kasemo, B.; Kall, M. Controlling plasmon line shapes through diffractive coupling in linear arrays of cylindrical nanoparticles fabricated by electron beam lithography. *Nano Lett.* **2005**, *5*, 1065−1070.

(19) Tseng, A. A. Recent developments in nanofabrication using focused ion beams. *Small* **2005**, *1*, 924−939.

(20) Ritala, M.; Leskela, M. Atomic layer epitaxy—a valuable tool for nanotechnology? *Nanotechnology* **1999**, *10*, 19−24.

(21) Frohlich, K.; Tapajna, M.; Rosova, A.; Dobrocka, E.; Husekova, K.; Aarik, J.; Aidla, A. Growth of high-dielectric-constant TiO_2 films in

capacitors with RuO_2 electrodes. *Electrochem. Solid-State Lett.* **2008**, *11*, G19−G21.

(22) Kim, H.; Lee, H. B. R.; Maeng, W. J. Applications of atomic layer deposition to nanofabrication and emerging nanodevices. *Thin Solid Films* **2009**, *517*, 2563−2580.

(23) George, S. M. Atomic Layer Deposition: An Overview. *Chem. Rev.* **2010**, *110*, 111−131.

(24) Profijt, H. B.; Potts, S. E.; van de Sanden, M. C. M.; Kessels, W. M. M. Plasma-Assisted Atomic Layer Deposition: Basics, Opportunities, and Challenges. *J. Vac. Sci. Technol., A* **2011**, *29*, 050801.

(25) Im, H.; Wittenberg, N. J.; Lindquist, N. C.; Oh, S. H. Atomic layer deposition: A versatile technique for plasmonics and nanobiotechnology. *J. Mater. Res.* **2012**, *27*, 663−671.

(26) Whitney, A. V.; Elam, J. W.; Zou, S.; Zinovev, A. V.; Stair, P. C.; Schatz, G. C.; Van Duyne, R. P. Localized surface plasmon resonance nanosensor: a high-resolution distance-dependence study using atomic layer deposition. *J. Phys. Chem. B* **2005**, *109*, 20522−20528.

(27) Im, H.; Lindquist, N. C.; Lesuffleur, A.; Oh, S. H. Atomic layer deposition of dielectric overlayers for enhancing the optical properties and chemical stability of plasmonic nanoholes. *ACS Nano* **2010**, *4*, 947−954.

(28) Aaltonen, T.; Ritala, M.; Sajavaara, T.; Keinonen, J.; Leskela, M. Atomic layer deposition of platinum thin films. *Chem. Mater.* **2003**, *15*, 1924−1928.

(29) Joo, S. H.; Choi, S. J.; Oh, I.; Kwak, J.; Liu, Z.; Terasaki, O.; Ryoo, R. Ordered nanoporous arrays of carbon supporting high dispersions of platinum nanoparticles. *Nature* **2001**, *412*, 169−172.

(30) Ko, C. T.; Han, Y. Y.; Chen, C. H.; Shieh, J.; Chen, M. J. Enormous Plasmonic Enhancement and Suppressed Quenching of Luminescence from Nanoscale ZnO Films by Uniformly Dispersed Atomic-Layer-Deposited Platinum with Optimized Spacer Thickness. *J. Phys. Chem. C* **2013**, *117*, 26204−26212.

(31) Baker, L.; Cavanagh, A. S.; Seghete, D.; George, S. M.; Mackus, A. J. M.; Kessels, W. M. M.; Liu, Z. Y.; Wagner, F. T. Nucleation and growth of Pt atomic layer deposition on Al_2O_3 substrates using (methylcyclopentadienyl)trimethylplatinum and O_2 plasma. *J. Appl. Phys.* **2011**, *109*, 084333.

(32) Jiang, X. R.; Huang, H.; Prinz, F. B.; Bent, S. F. Application of atomic layer deposition of platinum to solid oxide fuel cells. *Chem. Mater.* **2008**, *20*, 3897−3905.

(33) Christensen, S. T.; Elam, J. W.; Rabuffetti, F. A.; Ma, Q.; Weigand, S. J.; Lee, B.; Seifert, S.; Stair, P. C.; Poeppelmeier, K. R.; Hersam, M. C.; Bedzyk, M. J. Controlled Growth of Platinum Nanoparticles on Strontium Titanate Nanocubes by Atomic Layer Deposition. *Small* **2009**, *5*, 750−757.

(34) Novak, S.; Lee, B.; Yang, X. Y.; Misra, V. Platinum Nanoparticles Grown by Atomic Layer Deposition for Charge Storage Memory Applications. *J. Electrochem. Soc.* **2010**, *157*, H589−H592.

(35) Aberle, A. G. Surface passivation of crystalline silicon solar cells: A review. *Prog. Photovoltaics* **2000**, *8*, 473−487.

(36) Schmidt, J.; Merkle, A.; Brendel, R.; Hoex, B.; van de Sanden, M. C. M.; Kessels, W. M. M. Surface passivation of high-efficiency silicon solar cells by atomic-layer-deposited Al_2O_3. *Prog. Photovoltaics* **2008**, *16*, 461−466.

(37) Hoex, B.; Gielis, J. J. H.; de Sanden, M. C. M. V.; Kessels, W. M. M. On the c-Si surface passivation mechanism by the negative-charge-dielectric Al_2O_3. *J. Appl. Phys.* **2008**, *104*, 113703.

(38) Ozbay, E. Plasmonics: Merging photonics and electronics at nanoscale dimensions. *Science* **2006**, *311*, 189−193.

(39) Haes, A. J.; Zou, S. L.; Schatz, G. C.; Van Duyne, R. P. A nanoscale optical biosensor: The long range distance dependence of the localized surface plasmon resonance of noble metal nanoparticles. *J. Phys. Chem. B* **2004**, *108*, 109−116.

(40) Whitney, A. V.; Elam, J. W.; Zou, S. L.; Zinovev, A. V.; Stair, P. C.; Schatz, G. C.; Van Duyne, R. P. Localized surface plasmon resonance nanosensor: A high-resolution distance-dependence study using atomic layer deposition. *J. Phys. Chem. B* **2005**, *109*, 20522−20528.

(41) Sinton, R. A.; Cuevas, A. Contactless determination of current-voltage characteristics and minority-carrier lifetimes in semiconductors from quasi-steady-state photoconductance data. *Appl. Phys. Lett.* **1996**, *69*, 2510−2512.

(42) Sun, B. M.; Sheng, J.; Yuan, S. Z.; Zhang, C.; Feng, Z. Q.; Huang, Q. Industrially Feasible Casting-Mono Crystalline Solar Cells with PECVD AlO_x/SiN_x Rear Passivation Stack towards 19.6% Efficiency. *38th IEEE Photovoltaic Specialists Conference (PVSC)*, Austin, TX, June 3−8, 2012; IEEE: New York, 2012; pp 1125−1128.

(43) Saint-Cast, P.; Heo, Y. H.; Billot, E.; Olwal, P.; Hofmann, M.; Rentsch, J.; Glunz, S. W.; Preu, R. Variation of the layer thickness to study the electrical property of PECVD Al_2O_3/c-Si interface. *Energy Procedia* **2011**, *8*, 642−647.

(44) Lei, D.; Yu, X. G.; Song, L. H.; Gu, X.; Li, G. H.; Yang, D. R. Modulation of atomic-layer-deposited Al_2O_3 film passivation of silicon surface by rapid thermal processing. *Appl. Phys. Lett.* **2011**, *99*, 052103.

(45) Wang, W. C.; Lin, C. W.; Chen, H. J.; Chang, C. W.; Huang, J. J.; Yang, M. J.; Tjahjono, B.; Huang, J. J.; Hsu, W. C.; Chen, M. J. Surface Passivation of Efficient Nanotextured Black Silicon Solar Cells Using Thermal Atomic Layer Deposition. *ACS Appl. Mater. Interfaces* **2013**, *5*, 9752−9759.

(46) Langhammer, C.; Yuan, Z.; Zoric, I.; Kasemo, B. Plasmonic properties of supported Pt and Pd nanostructures. *Nano Lett.* **2006**, *6*, 833−838.

(47) Suzuki, T.; Miyata, H.; Noma, T.; Kuroda, K. Platinum thin film consisting of well-aligned nanowires and its optical behavior. *J. Phys. Chem. C* **2008**, *112*, 1831−1836.

(48) Ameling, R.; Giessen, H. Microcavity plasmonics: strong coupling of photonic cavities and plasmons. *Laser Photonics Rev.* **2013**, *7*, 141−169.